JACS
JOURNAL OF THE AMERICAN CHEMICAL SOCIETY

Article

pubs.acs.org/JACS

New Models of Tetrahymena Telomerase RNA from Experimentally Derived Constraints and Modeling

Daud I. Cole,[†,§] Jason D. Legassie,[‡,§] Laura N. Bonifacio,[‡,§] Vijay G. Sekaran,[‡] Feng Ding,[†,○] Nikolay V. Dokholyan,*[,†] and Michael B. Jarstfer*[,‡]

[†]Department of Biochemistry and Biophysics, School of Medicine, and [‡]Division of Chemical Biology and Medicinal Chemistry, Eshelman School of Pharmacy, University of North Carolina at Chapel Hill, Chapel Hill, North Carolina 27599, United States

Supporting Information

ABSTRACT: The telomerase ribonucleoprotein complex ensures complete replication of eukaryotic chromosomes. Telomerase RNA (TER) provides the template for replicating the G-rich strand of telomeric DNA, provides an anchor site for telomerase-associated proteins, and participates in catalysis through several incompletely characterized mechanisms. A major impediment toward understanding its nontemplating roles is the absence of high content structural information for TER within the telomerase complex. Here, we used selective 2′-hydroxyl acylation analyzed by primer extension (SHAPE) to examine the structure of *Tetrahymena* TER free in solution and bound to tTERT in the minimal telomerase RNP. We discovered a striking difference in the two conformations and established direct evidence for base triples in the tTER pseudoknot. We then used SHAPE data, previously published FRET data, and biochemical inference to model the structure of tTER using discrete molecular dynamics simulations. The resulting tTER structure was docked with a homology model of the *Tetrahymena* telomerase reverse transcriptase (tTERT) to characterize the conformational changes of tTER telomerase assembly. Free in solution, tTER appears to contain four pairing regions: stems I, II, and IV, which are present in the commonly accepted structure, and stem III, a large paired region that encompasses the template and pseudoknot domains. Our interpretation of the data and subsequent modeling affords a molecular model for telomerase assemblage in which a large stem III of tTER unwinds to allow proper association of the template with the tTERT active site and formation of the pseudoknot. Additionally, analysis of our SHAPE data and previous enzymatic footprinting allow us to propose a model for stem-loop IV function in which tTERT is activated by binding stem IV in the major groove of the helix-capping loop.

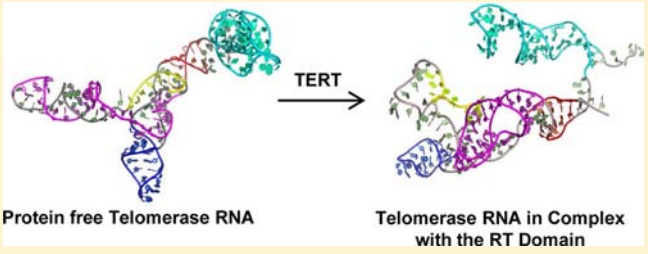

INTRODUCTION

Ribonucleic acid has vast functions beyond its canonical roles in the transcription and translation of genetic information.[1] Many of these functions require specific RNA folding, and like proteins, many RNAs fold into complex three-dimensional structures that are essential for their function.[1,2] Generally, RNAs are considered more conformationally dynamic than proteins, in part because RNAs possess six backbone torsion angles rather than three backbone torsion angles present in peptides.[3] A detailed understanding of RNA function therefore requires a description of both the RNA tertiary structure as well as the major available alternative conformations. However, many larger RNAs, particularly those in ribonucleoprotein complexes (RNPs), are challenging to study by X-ray crystallography or NMR. To overcome this problem, computational methods using experimental constraints afford an approach toward obtaining high-resolution structural models as well as assessing conformational flexibility of RNAs.

Telomerase is an important RNP for which high-resolution structural data of the RNA within the RNP remain incomplete.[4] In fact, no structural data of an intact, minimally functional telomerase complex have been reported except for low-resolution electron microscopic analysis of telomerase isolated from *Euplotes aediculatus*.[5] Telomerase elongates the linear chromosomes of most eukaryotes with repeating sequences of guanosine-rich DNA to solve the end replication problem faced during DNA replication.[6] Telomerase is critical for the genomic integrity of dividing cells because of its central role in maintaining the chromosome ends. Mutations that disrupt telomerase function have been linked to several genetic disorders such as dyskeratosis congenita and idiopathic pulmonary fibrosis,[7] and telomerase activity is elevated in cancer cells.[8] The importance of telomerase activity in many human disease states suggests that the detection and control of telomerase may prove to be effective diagnosis and treatment strategies.[9] However, the incomplete understanding of telomerase structure and catalytic mechanism hinders the rational design of effective telomerase-based therapies.

Telomerase RNPs demonstrate rapid evolutionary divergence, but all minimally contain a catalytic subunit, telomerase reverse transcriptase (TERT), and a RNA subunit, telomerase

Received: June 20, 2012
Published: November 19, 2012

   dx.doi.org/10.1021/ja305636u | *J. Am. Chem. Soc.* 2012, 134, 20070−20080

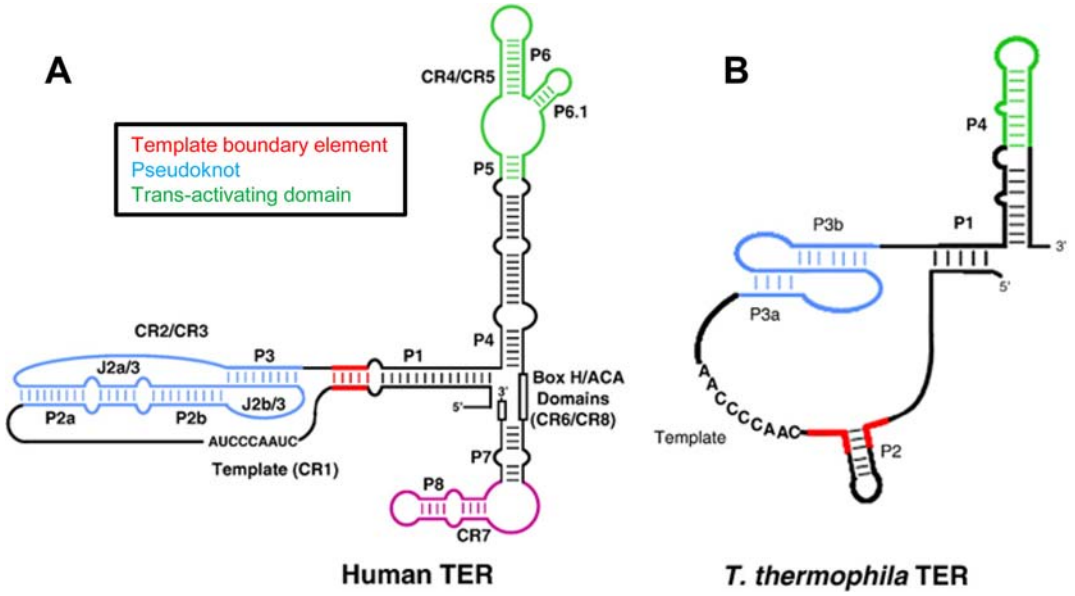

Figure 1. Cartoon of (A) human and (B) Tetrahymena telomerase RNA.

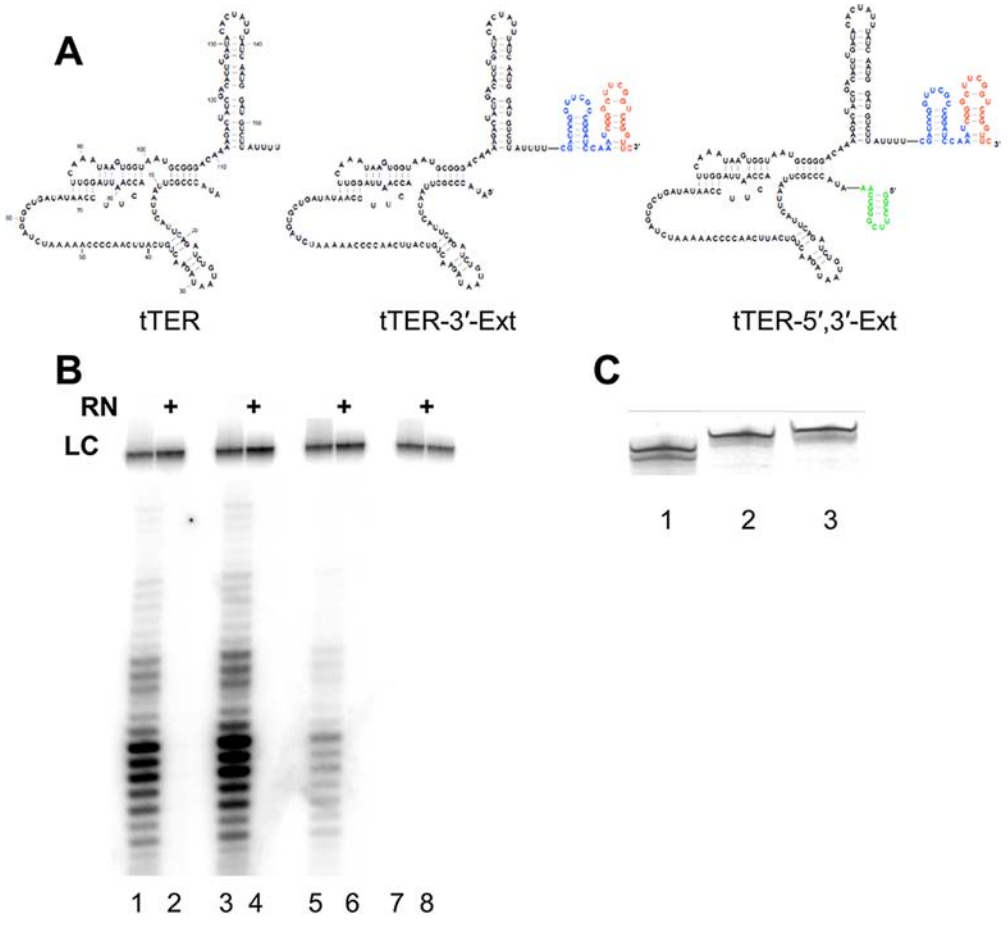

Figure 2. A tTER construct for SHAPE experiments. (A) Wild-type tTER is shown together with tTER-3′-Ext and tTER-5′,3′-Ext. The 3′-extensions include a linker (blue) and a primer binding site (red). The 5′-extension is indicated in green. The extensions facilitate analysis of the entire RNA by reverse transcription. (B) Activity of telomerase reconstituted with tTERT and wild-type tTER (lanes 1 and 2), tTER-3′-Ext (lanes 3 and 4), tTER-5′,3′-Ext (lanes 5 and 6), or no RNA (lanes 7 and 8). RN indicates treatment with RNase A prior to conducting telomerase assays. LC indicates a ^{32}P-labeled, 100 nucleotide loading control. Telomerase was assayed by primer extension as described in methods. (C) Analysis of in vitro transcribed tTER constructs by denaturing gel electrophoresis. Lane 1, wild-type; lane 2, tTER-3′-Ext; lane 3, tTER-5′,3′-Ext.

RNA (TER).[10] TERT is conserved in telomerase-containing species and contains several highly conserved domains including RNA-binding and reverse transcriptase domains. TERs are not well conserved but do share functionally related

dx.doi.org/10.1021/ja305636u | J. Am. Chem. Soc. 2012, 134, 20070−20080

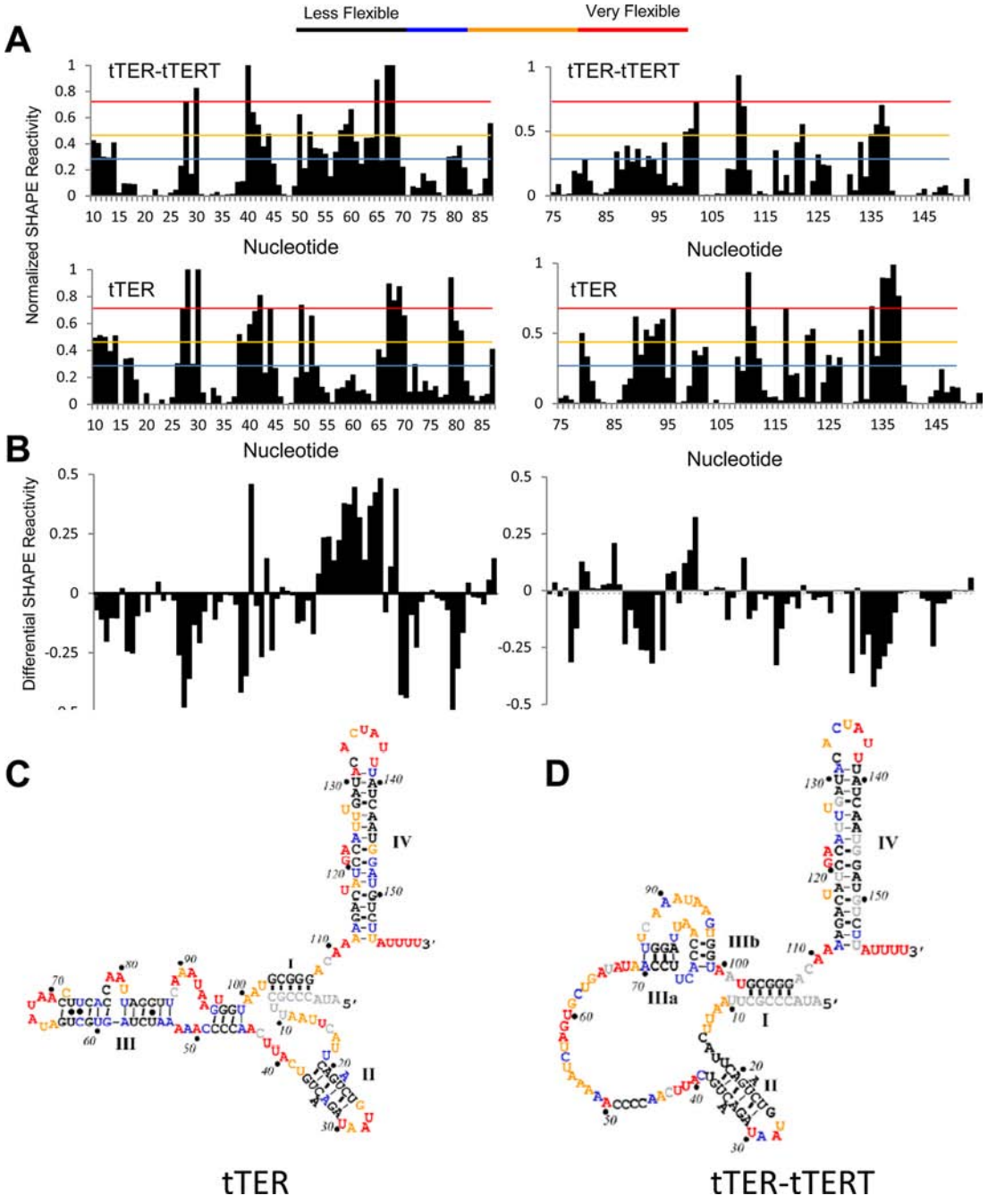

Figure 3. SHAPE analysis of tTER in solution and bound to tTERT. (A) Quantified data from SHAPE experiments were plotted versus nucleotide position. (B) Differential plot of SHAPE reactivities: tTER−tTERT minus free tTER reactivities. (C) Secondary structure of free tTER color coded for SHAPE reactivity. The structure was generated using *RNAstructure*. (D) Secondary structure of tTER bound to tTERT color coded for SHAPE reactivity. Stems I, II, and IV were generated using *RNAstructure*. The base-paring of the pseudoknot region was set manually. See Figure S1 of the Supporting Information for representative raw data.

domains: a template, a pseudoknot adjacent to the template, and a trans-activating domain that enhances catalytic activity in what appears to be an allosteric fashion.[11] Telomerase from the ciliate *Tetrahymena thermophila* has served as an important model since its activity was first detected,[12] and it can be reconstituted in vitro using rabbit reticulocyte lysates and recombinant *Tetrahymena* TERT and TER.[13] *Tetrahymena* TER (tTER) is 159 nucleotides long and contains the functionally conserved TER domains.[14] In addition to these, tTER has several well-characterized domains that contribute to RNP assemblage and biochemical activity (Figure 1). Endogenous telomerase RNPs generally contain an RNA-binding protein required for biogenesis and stability of the complex.[15] In humans, this activity is supplied by the box H/ACA-binding protein dyskerin.[16] In Tetrahymena, the core telomerase RNP contains the specific tTER-binding protein p65.[17] In vitro, the efficiency of telomerase assemblage is enhanced by p65 because of its apparent ability to facilitate conformational changes in tTER and stabilize the active conformation.[18]

Telomerase exhibits several unique structural and biochemical features. Unlike most reverse transcriptases, telomerase

dx.doi.org/10.1021/ja305636u | J. Am. Chem. Soc. 2012, 134, 20070−20080

appears remarkably specific for the template embedded in its RNA subunit, and the RNA subunit also appears to activate telomerase activity through poorly understood mechanisms.[14c] Although there is some evidence that TERT can utilize alternative templates, this alternative activity appears much less efficient than its canonical acticty.[19] Like all reverse transcriptases, telomerase catalyzes processive nucleotide addition to its primer. Uniquely, telomerase also efficiently conducts repeat addition processivity to generate long copies of its repetitive DNA product.[20] TER therefore must exist in multiple conformations throughout the catalytic cycle, and these conformations are constrained by RNA−RNA, RNA−DNA, and RNA−protein interactions. Accurate descriptions of these interactions in the minimal telomerase complex and at discrete steps of catalysis remain elusive. To date, the structures of ciliate and vertebrate TERs within the telomerase complex have been suggested on the basis of phylogenetic comparative analysis,[21] and many aspects of these models have been validated experimentally.[14a]

We sought to better understand the three-dimensional structure and conformational changes associated with tTER function within the telomerase RNP. We combined secondary structural constraints of tTER obtained using the high-resolution footprinting technique selective 2′-hydroxyl acylation analyzed by primer extension (SHAPE),[22] distance constraints obtained from single-molecule FRET data,[18b] and biochemical inference gleaned from previous biochemical experiments to generate constraints. We then modeled the structure of tTER in the minimal complex using discrete molecular dynamics (DMD) that allows facile incorporation of experimental information.[23] In addition, we docked the resulting model with a homology model of tTERT based on the crystal structure of the *T. Castaneum* TERT[24] and the tTERT RNA binding domain[25] to generate a three-dimensional model of tTER in the minimal telomerase complex. The results reveal conformational changes that occur during telomerase assembly and suggest a model for stem IV binding to tTERT.

RESULTS

A Recombinant Telomerase Complex for Chemical Probing Experiments. Because accurate structural modeling requires robust experimental constraints, we generated quantifiable data reporting on individual tTER nucleotides using SHAPE chemistry.[22] SHAPE chemistry measures the reactivity of RNA 2′-hydroxyl groups with isatoic anhydride derivatives. Reactivity is primarily governed by nucleotide flexibility with more flexible nucleotides exhibiting greater reactivity.[26] Nucleotide acylation was mapped as reverse transcription stops. To maximize coverage of tTER in SHAPE experiments, we added a 3′-extension with a primer binding site for reverse transcription and a linker that separated the primer binding site from tTER to generate tTER-3′-Ext (Figure 2). We confirmed that the extension allowed reconstitution of active telomerase and conducted SHAPE experiments on tTER-3′-Ext in the presence and absence of tTERT.

In Vitro Transcribed Tetrahymena Telomerase RNA Forms an Extended Stem III Instead of a Stem IIIa/IIIb Pseudoknot. We used *N*-methylisatoic anhydride (NMIA) to generate the SHAPE profile of tTER-3′-Ext in the absence of tTERT (Figures 3 and S1). We quantified SHAPE reactivities for 149 of the 159 tTER nucleotides, and the data were used to constrain predictions using the program *RNAstructure*.[27] Remarkably, the secondary structure of tTER using SHAPE data contained all but four of the base pairs predicted by *RNAstructure* using only the primary sequence.[27] Both the SHAPE constrained and the unconstrained models of protein-free tTER contained many features present in the currently accepted secondary structure model of tTER including stems I, II, and IV. The most prominent difference was in the template and pseudoknot domains, which included a large stem III that encompassed several template residues instead of the stem IIIa/IIIb pseudoknot (Figure 3). To ensure that the 3′-extension did not perturb the native tTER structure leading to the formation of the large stem III confirmation, we compared both the SHAPE and the RNase V1 profiles of wild-type tTER to tTER-3′-Ext. We detected no difference in the footprinting profiles of the RNAs, and interpretation of the SHAPE data by *RNAstructure* generated the same secondary structures for tTER and tTER-3′-Ext (Figure S2 and data not shown).

We compared the SHAPE data to reported NMR structures and found excellent agreement (Figure S3).[28] The SHAPE profile for stem IV correlates with the generalized order parameter S^2, consistent with previously reported data for a small stem IV model,[29] and is consistent with the stem IV solution structure, as we previously reported.[28a] SHAPE reactivity of stem II also correlated with its solution structure. Each nucleotide forming the predicted stem II helix was unreactive to NMIA, including A22 and A34. This suggests that A22 and A34 are stacked within the helix and not bulged as is typically drawn, consistent with NMR data.[28b] Interestingly, the loop residues of stem II exhibited mixed levels of reactivity. G26 and A29 were less reactive than A28 and U30, suggesting that G26 and A29 are structured despite residing in a single-stranded loop. Indeed, the solution structure indicates that stem II is capped by a structured pentaloop with G26 stacked on top of the terminal U25-A31 base pair and A29 is tucked into the pentaloop structure. We conclude that the previously reported solution structure of stems II and IV accurately represent these domains in full-length tTER.

Surprisingly, the SHAPE profiles of the template and pseudoknot nucleotides (nts 45−99) are inconsistent with the accepted secondary structure of tTER. Instead, the data suggest with high probability that these nucleotides are involved in a large and stable stem-loop structure. This model is remarkably consistent with previous footprinting data,[11b,18a,30] but the SHAPE experiment revealed sufficient constraints to confidently make this conclusion (Table S2). Moreover, recently reported FRET data also suggest that a pseudoknot does not form in protein-free tTER due to disruptive interactions with other parts of the RNA.[31] These interactions now appear defined. Instead of a pseudoknot and single-stranded template region, the pseudoknot and template nucleotides participate in extensive base pairing to form an extended stem III (Figure 3C).

TERT Induces a Conformational Change in tTER. The structure of in vitro transcribed tTER we determined is incompatible with a functional telomerase RNP as it would prevent association of the template with the active site. We therefore predicted that binding to tTERT would result in significant conformational changes in the template and pseudoknot domains of tTER. To test this hypothesis, we assembled telomerase in rabbit reticulocyte lysates, immunopurified the complex, and analyzed the structure of tTER by SHAPE. We posited that acylation by a SHAPE reagent might destabilize the telomerase complex and compromise the

dx.doi.org/10.1021/ja305636u | J. Am. Chem. Soc. 2012, 134, 20070−20080

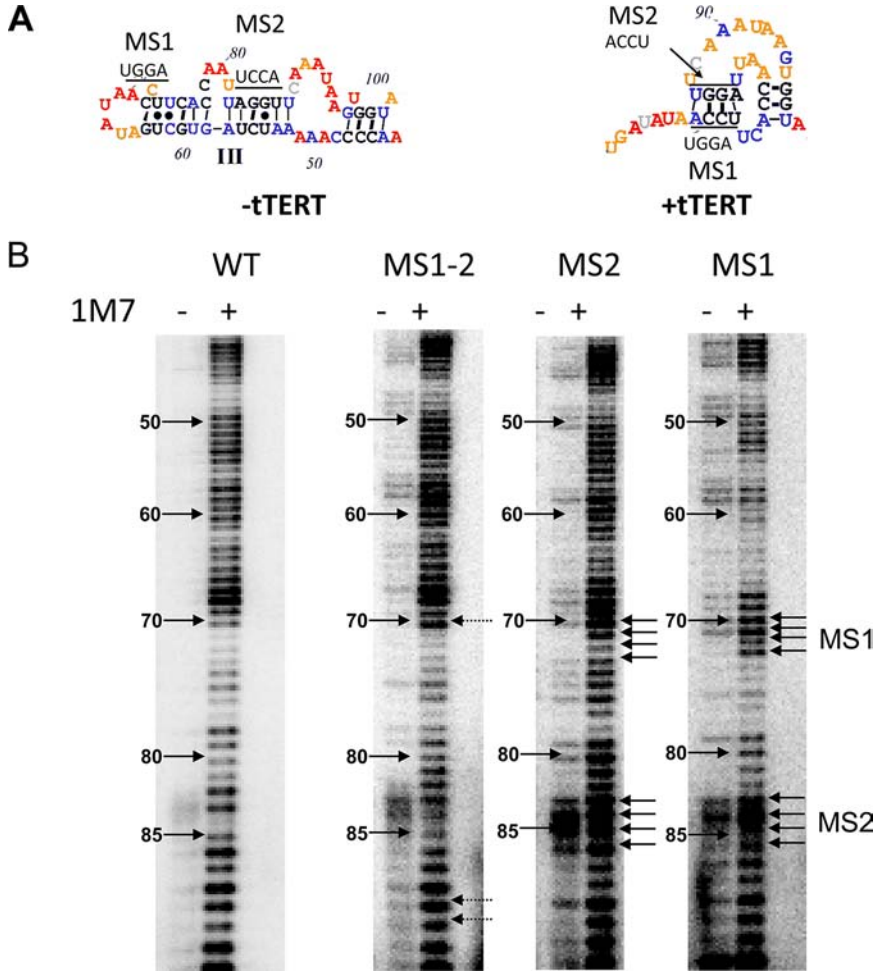

Figure 4. Mutational analysis of tTER provides evidence for base-pairing interactions in the stem III pseudoknot. (A) Positions of mutations in tTER are indicated. (B) SHAPE analysis of tTER mutants in complex with tTERT. Arrows indicate positions of the MS1 and MS2 mutations.

experiments. This concern was validated by demonstrating that acylation with NMIA was destabilizing to telomerase complex (Figure S4). For our studies, we therefore performed SHAPE on the telomerase complex for 1 reagent half-life to maximize signal-to-noise and avoid potential contribution of tTER that has dissociated from tTERT. We also confirmed that the SHAPE reactivity profile of tTER in the tTERT complex was not time dependent over the course of the experiments (Figure S5).

A histogram of all SHAPE reactivities for free tTER as compared to reactivities of tTER bound to TERT shows no appreciable difference in the overall distribution of specific SHAPE values between the two conditions: an equal number of nucleotides became more reactive to the SHAPE reagent as became less reactive when tTER was bound to TERT. However, we observed significant localized SHAPE-reactivity changes in TERT-bound tTER when compared to protein-free tTER (Figures 3 and S1). Remarkably, nucleotides exhibiting increased reactivity were concentrated from A53-G65: the template recognition element and proposed tTERT binding site 3′ of the template. In the absence of tTERT, these nucleotides are resistant to NMIA. However, upon assembly they become SHAPE reactive, suggesting they become single stranded upon binding to tTERT.

Nucleotides with decreased SHAPE reactivity were present in provocative locations: the residues flanking the base of stem II, the loops of stems II and IV, and nucleotides that constitute the presumed pseudoknot stems IIIa and IIIb: A69−C72, A79−A80, and A89−U96. The SHAPE profiles of stems II and IV are consistent with reported solution structures, including correlation of S^2 for stem IV nucleotides.[29] Nucleotides predicted to be base paired demonstrated low SHAPE reactivity while loop nucleotides displayed mixed SHAPE reactivity. Notably, nucleotides predicted to be ordered by NMR displayed low SHAPE reactivity.[28] These observations further validate the solution structures as accurate models of these domains in the functional telomerase RNP.

Predictions of tTER Base Pairing. We utilized the folding algorithm *RNAstructure* to predict base-pairing probability for tTER nucleotides and compared these predictions to the tTER model based on comparative sequence analysis (CSA model).[27] The currently accepted tTER model contains 40 base pairs, including 13 in the pseudoknot region.[30,32] Stems I, II, and IV contribute 27 of these 40 base pairs. *RNAstructure* predicted the 27 base pairs in stems I, II, and IV without experimental constraints. The five base pairs in stem I are predicted without the aid of SHAPE constraints to exist with probabilities exceeding 99%. The six base pairs in stem II are all predicted with probabilities exceeding 95%. Fourteen of the 16 base pairs in stem 4 are predicted with probabilities exceeding 80%. Both MaxExpect[33] and ProbKnot[34] predict U126 and U127 to base pair with A144 and A143 respectively instead of U126 and

dx.doi.org/10.1021/ja305636u | J. Am. Chem. Soc. 2012, 134, 20070−20080

U125. The U126−A144 base pair is predicted with 45% probability, while the U127−A143 pair is predicted with 86% (Figure S6).

We incorporated the SHAPE intensities of tTER in complex with tTERT into *RNAstructure* predictions. *RNAstructure* predicted 32 of the 40 tTER base pairs present in the CSA model (sensitivity of 80%), and 32 of the 38 base pairs in *RNAstructure* model are found in the CSA model (positive predictive value of 84%). All of the 27 base pairs in stems I, II, and IV of the CSA model were predicted. Additionally, the five base pairs in stem IIIA of the putative pseudoknot in the CSA model were also correctly predicted. However, stem IIIb of the pseudoknot in the CSA model was not present in predictions. Instead, structures included long-range base-pairs between nucleotides 94−98 and 14−18. This long-range interaction is not consistent with the biochemical understanding of telomerase and likely results from the inability of *RNAstructure* to accurately predict the tTER pseudoknot (Figure S7). Because the pseudoknot domain was not accurately predicted, we compared the SHAPE profiles to several possible pseudoknot structures including the CSA model,[30,32] a model predicted by the Tzfati lab,[35] and models predicted by several heuristic algorithms (Figure S8).[36] In no case was the SHAPE profile completely consistent with the predicted base-pairing pattern. Overall, only two sets of base-pairing interactions are consistently supported by predictions and the SHAPE data: 70-ACCU/83-AGGU and 76-ACC/97-GGU.

Test of Predicted Stem IIIa Base Pairs by SHAPE and Activity Analysis of tTER Mutants. We designed three mutants to test the proposed protein-free and tTERT-bound tTER models. Mutants were designed to deferentially affect the stability of stem III in the protein-free model and stem IIIa in the tTERT-bound model (Figure S9). The models predict that two mutants, MS1 (70-ACCU → 70-UGGA) and MS2 (83-AGGU → 83-UCCA), would alter several base-pairing interactions in both protein-free and tTERT-bound tTER, whereas double mutant MS1/MS2 is predicted to dramatically destabilize the protein-free structure but allow base pairing in the tTER complex due to the compensatory mutations. SHAPE profiles of protein-free MS1, MS2, and MS1/MS2 suggest disruption of the wild-type tTER stem III structure and new but poorly formed structures or mixtures of several structures (Figure S9). Importantly, the SHAPE profile of protein-free MS1/MS2 was distinct from wild-type, protein-free tTER consistent with the hypothesis that these residues are not associated by base pairing.

When bound to tTERT, MS1 exhibited a shift in SHAPE reactivity, making it appear to have formed a new structure (Figure 4). We examined possible secondary structures of the MS1 pseudoknot using heuristic modeling algorithms and found that several stable pseudoknot structures are compatible with the MS1 sequence and SHAPE reactivity of MS1 bound to tTERT. MS2 exhibited a much greater increase in SHAPE reactivity of both the mutated residues as well as their predicted base-pairing partners. Unlike MS1, none of the algorithms we tested predicted a stable structure for an MS2 pseudoknot. In striking contrast to protein-free tTER, the SHAPE profile of MS1/MS2 is nearly indistinguishable from the profile of wild-type tTER. Notable exceptions include A70 and A90, which exhibited increased reactivity in the MS1/MS2 mutant when compared to wild-type tTER. We examined the effect of disrupting predicted base-pairs in stem IIIa on telomerase activity and found that both MS1 and MS2 exhibited severely reduced telomerase activity, while MS1/MS2 retained wild-type activity (Figure 5). It should be pointed out that similar mutations, 71-CC → 71-GG and 84-GG → 84-CC, were reported to show decreased telomerase activity that can be rescued by p65.[18a]

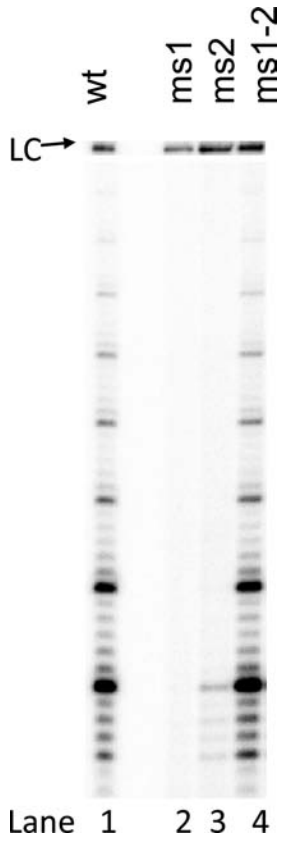

Figure 5. tTER mutants that disrupt base pairing in the pseudoknot prevent reconstitution of robust telomerase activity. Telomerase activity of the tTERT−tTER minimal complex was determined by direct primer extension. LC indicates a loading control used for normalization.

DMD Analysis of tTER. DMD simulations have been successfully used to model the three-dimensional structures of RNAs, and the accuracy of modeling can be greatly enhanced by experimental constraints.[23,37] We performed DMD simulations to generate structural models of protein-free and tTERT-bound tTER using both SHAPE-derived secondary structure and FRET-derived distance constraints (Figure S10).[23] Protein-free tTER formed the predicted pairing regions stems I, II, and IV present in the CSA as well as the large stem III predicted by SHAPE constrained *RNAstructure*. In exploratory studies, initial models of tTERT-bound tTER generated with SHAPE and FRET data alone exhibited long-range base pairing like that found using *RNAstructure* (see Figure S7) that would block a proposed tTERT binding site as well as seemingly preclude proper association of the template with the tTERT active site. We therefore included several constraints based on biochemically inference (Figure S11). First, we introduced a nine-nucleotide RNA sequence that was complementary to tTER template nucleotides 43−51 to mimic association of tTER with its primer and provide a steric block of the template from other tTER domains. Because nucleotides 15−18 are predicted to function as a protein binding site,[38] we

dx.doi.org/10.1021/ja305636u | J. Am. Chem. Soc. 2012, 134, 20070−20080

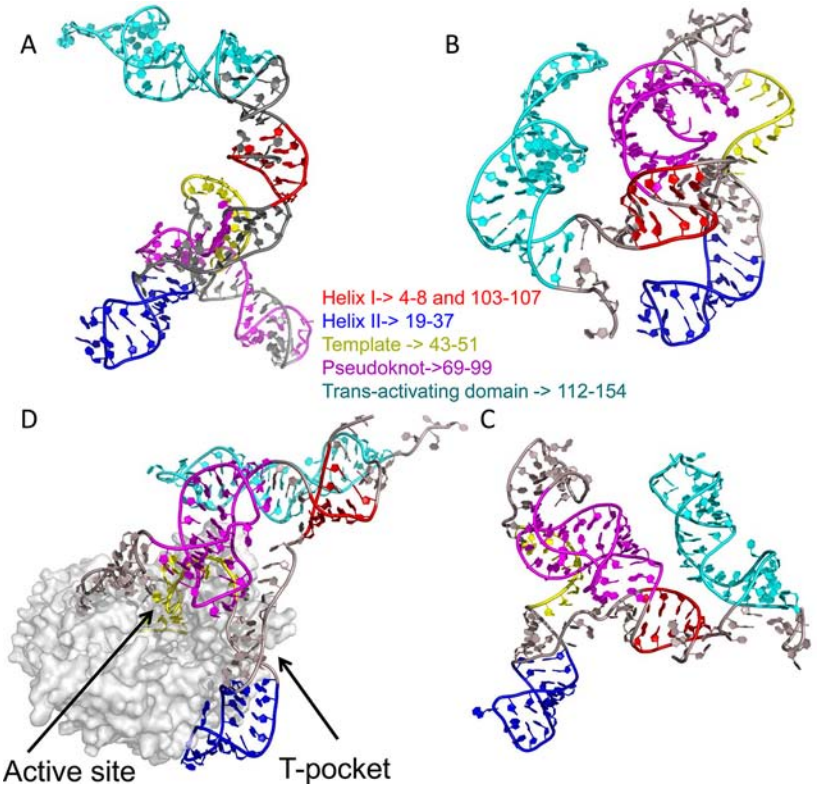

Figure 6. Conformations of tTER free in solution and bound to tTERT. tTER was modeled using DMD simulations using constraints describe in the Materials and Methods. (A) Unbound tTER. (B and C) The two most extreme populations of tTER bound to tTERT predicted by DMD. (C) The most populated state. (D) The structure of tTER predicted by DMD when docked to a homology model of tTERT. The TEN domain and flexible linker to the reverse transcriptase domain of TERT were not modeled. Three DNA substrate nucleotides buried within the active site in very close proximity to the catalytic triad of aspartates are colored yellow. The T-pocket of the RNA binding domain of tTERT is indicated. All tTER models are aligned along stem IV nucleotides. Telomerase RNA is shown with stem I nucleotides colored red, stem II nucleotides colored blue, template nucleotides colored yellow, pseudoknot nucleotides colored magenta, and stem IV nucleotides colored cyan. All remaining nucleotides are colored gray.

also restricted the distances between tTER nucleotides 10−18 and the rest of the RNA to no less than 10 Å to ensure these nucleotides remain single-stranded. The resulting models recapitulate all of the established base pairs in stems I, II, and IV. The models also predicted the stacked adenosines 22 and 34 of stem II, consistent with models from NMR data.[28b] Cluster analysis of tTER folding trajectories, which identifies distinct conformational states sampled in simulations, revealed three stable domains that are internally stable: a region encompassing stem IV (nucleotides 112−159), a region encompassing the template (nucleotides 1−107), and a flexible linker between stem IV and stem I (108−111). In the simulations, the flexible linker allows stem IV and the template domains of tTER to change coordinates with respect to each other. Examination of the representative structures from cluster analysis indicates that movement in the flexible linker region enables the template nucleotides 43−51 to rotate approximately 90° in relation to stationary stem IV. This suggests that the template nucleotides 43−51 can exist in several discrete positions with respect to stem IV.

One aspect of the DMD-generated models that did not appear to allow tTER function in the telomerase complex was the close association of the template with the rest of the RNA (Figure 6B and C). We therefore modeled tTER bound to a homology model of tTERT. To constrain tTER binding, we aligned the template to the coordinates of a DNA primer available from the *T. castaneum* TERT crystal structure, which contains a model of the predicted *T. castaneum* telomerase template RNA residues base paired to the complementary DNA contained in a chimeric hairpin.[24] We performed DMD simulations to relax tTER while maintaining the secondary and tertiary structures of tTER. As we expected, docking to the tTERT model as a constraint altered the tTER structure (Figure 6D). The major change was a twist in the template-containing strand away from the remainder of tTER commensurate with extending stem II away from the main body of the RNA. The tTER model contains stems I, II, IIIa/IIIb, and IV with stem IV pointed toward the IIIa/IIIb pseudoknot. The template recognition element and the template are positioned away from the main body of tTER to accommodate association with the tTERT active site. The stem II model aligns within 1.5 Å root-mean-square deviation (RMSD) of the published NMR structure,[28b] and stem IV aligns to within 5.4 Å RMSD of the published NMR structure (Figure S12).[28a,c]

DISCUSSION

Binding to tTER Causes a Major Conformational Change in tTER. We combined SHAPE chemistry, published FRET, and molecular modeling to examine the three-dimensional structure of tTER. By comparing unbound tTER to tTER in the minimal telomerase complex, we revealed a dramatic conformational change in tTER that attends assemblage in the minimum telomerase complex. The most

dx.doi.org/10.1021/ja305636u | J. Am. Chem. Soc. 2012, 134, 20070−20080

noteworthy evidence for the conformational change is indicated by the SHAPE profile for nucleotides A53−A100, which includes the template recognition element and presumed pseudoknot domain (Figure 3). We interpret this change as evidence for the absence of a pseudoknot in protein-free tTER and formation of a pseudoknot in tTERT-bound tTER.

The SHAPE-inferred secondary structure of tTER in solution is remarkably different from the accepted secondary structure associated with tTER function in that the template and pseudoknot form a large paired region that we refer to as stem III. Importantly, this model is consistent with previous enzymatic and chemical footprinting of tTER (Table S1). It is notable that previous tTER structure probing experiments did not lead to the protein-free structure of tTER we predict. In part, this is a result of insufficient data available to accurately assign the structure. Recent experiments using RNase One do provide wider coverage, and RNase One is reported to cleave single-stranded RNA.[18a] It is surprising then that the reactivity profile of protein-free tTER using RNase One varies so much from SHAPE reactivity, particularly in the stem III domain of the protein-free structure (residues A44−U102, see Table S1). This difference requires an explanation. One possibility for decreased RNase One reactivity at nonbase-paired nucleotides is steric restriction on RNase One binding. Additionally, RNase One binding could shift the structural equilibrium from double-stranded to single-stranded RNA. This would result in increased reactivity at base-paired residues. Because SHAPE is governed almost exclusively by flexibility, these secondary effectors of RNase One reactivity may explain the differences between SHAPE and RNase One and would challenge accurate structural interpretation of RNase One experiments when compared to SHAPE chemistry. The model proposed here for the protein-free tTER structure also rationalizes FRET data of tTER at labeled pairs U63 and U92 and pairs U73 and U99 that are lower than expected for a folded pseudoknot.[31] The FRET data are, however, consistent with an extended stem III structure.

The SHAPE-inferred secondary structure of tTER bound to tTERT, in contrast to the protein-free structure, is consistent with the accepted secondary structure. However, the specific base-pairing pattern of the pseudoknot domain remains challenging to define. In an attempt to better address this, we compared the SHAPE profile of the pseudoknot residues with several proposed models (Figure S8). We found that not one model was entirely consistent with the SHAPE profile; instead, each model is partially consistent with the data. The G−C-rich regions are predicted by each model to be base-paired, which is consistent with the SHAPE profile. However, the A−U-rich regions do not appear to form a consistent base-pairing pattern. It seems that the pseudoknot domain forms a triple helix with the reactive A−U-rich nucleotides bound to the minor or major groove of stems IIIa and IIIb, similar to the model forwarded by the Tzfati lab.[35] To account for the high SHAPE reactivity of the A−U-rich strands of the pseudoknot domain, we propose that either several base-pairing configurations of the pseudoknot are present or the pseudoknot is flexible. One possibility is that during catalysis or in the presence of the telomerase holoenzyme component p65, the pseudoknot forms a more stable structure.

The decrease in SHAPE reactivity of the apical loops of stem-loops II and IV upon binding tTERT is evidence for decreased flexibility resulting from either increased stability of the secondary structure elements or direct tTERT interaction. Specifically, the loop of stem II that displayed decreased SHAPE reactivity is unlikely to bind directly to tTERT because mutating or extending the length of stem II is well tolerated.[18b,39] Accordingly, we conclude that association of tTER with tTERT stabilizes stem II resulting in decreased nucleotide flexibility. The reduced reactivities of 15-CAUU-18 and 39-UC-40 are consistent with predicted direct and stable interactions of these nucleotides with tTERT. Binding to tTERT could reduce nucleotide flexibility or sterically block reaction with NMIA.

Like stem-loop II, stem-loop IV residues displayed decreased SHAPE reactivity within the loop region. Several previous reports suggest a direct interaction between loop IV and tTERT. Therefore, direct interactions with tTERT as well as increased structural order are likely to contribute to the observed decrease in SHAPE reactivity. Interestingly, RNase One was reported to display the opposite distribution of reactivities in loop IV with A136, U137, and U138 exhibiting resistance to RNase One cleavage but high SHAPE reactivity (Table S2). One model that is consistent with the data is that residues C132, A133, and C134 form a rigid platform to constrain the range of motion of flexible nucleotides 135-UAUU-138. Evidence from several mutagenesis studies suggests that stem IV binds tTERT and that this interaction is stabilized by p65. Interestingly, when the C132−U138 base pair is mutated to an A−U base pair, SHAPE reactivity decreases for U138 commensurate with dramatically reduced catalytic activity.[28a] Flexibility in these nucleotides therefore seems in part related to their biochemical role in telomerase assembly. Interestingly, mutation of A136, U137, and U138 causes a significant decrease in assembly of active telomerase even in the presence of p65, but does not appear to negatively affect activity of properly assembled complexes. We propose that the UAUU nucleotides are flexible to allow an induced fit with tTERT. In addition, we predict that tTERT binds tTER in the major groove of stem IV. Binding the major groove would likely protect A136, U137, and U138 from RNase One cleavage but not block reaction of these nucleotides with NMIA, assuming RNase ONE cleavage is governed by sterics and NMIA by nucleotide flexibility.

We were surprised that four template residues, 46-CCCC-49, remained resistant to SHAPE reactivity after assembly. These nucleotides are also resistant to RNase One cleavage when tTER is bound to the N-terminus of tTERT (amino acids 1−516). Because a primer must bind these residues, we expected that they were single stranded and would exhibit high SHAPE reactivity. The low reactivity suggests that these nucleotides are directly bound to tTERT in a rigid conformation in the active site, perhaps providing a platform for primer binding.

A Three-Dimensional Model of tTER. The three-dimensional model of tTER generated by DMD simulations predicts all base pairs within stems I, II, and IV and displays relatively low RMSD alignments to NMR-generated models of stems II and IV. Although the biochemical data do not allow assignment of a specific base-pairing pattern for the pseudoknot, DMD simulation suggests a compact structure with several base triples. The DMD simulations also allow insight into tTER dynamism. Overall, simulations reveal that the template region is remarkably flexile (compare Figure 6B, C to D). The simulations suggest that one important aspect of this flexibility is rotation of the single-stranded region between stems I and IV. One possibility is that the lack of FRET constraints for any nucleotides in the distal loop of the stem II

domain may account for this dynamic positioning of the template. An alternative and more interesting interpretation is that the observed motion captures necessary movement of the template during successive rounds of nucleotide addition and repeat addition processivity. On the basis of this model, stem IV remains docked to tTERT in an allosteric activating site while the template can cycle through its required positions, a motion allowed by rotation about the linker between stem IV and stem I (Figure 6) perhaps coupled with scrunching of the template recognition element.[40] Alternatively, the motion may allow proper docking of stem IV during assemblage.

A Biological Model for the tTER Structural Rearrangement. The significant conformational change we detected in tTER that attends telomerase assemblage can be interpreted in many ways. One possibility is that the alternative structure is an artifact of in vitro transcription, and tTER does not fold into a biologically relevant structure due to the lack of tTER-binding partners, for example p65, which may be present during its transcription in vivo. Alternatively, it can be proposed that tTER folds as we show for the protein-free tTER in vivo prior to p65 binding, which can induce a conformational change in tTER,[18] followed by association with tTERT. If this is the case, does the misfolded tTER structure serve a purpose? We propose a model that protein-free tTER folds with a large stem III to sequester the template cytosine residues in a double stranded helix until assembly to protect the integrity of the telomere sequence and may serve other purposes as well. Because tTER codes for the DNA sequence at chromosome termini, damage to the templating residues could have significant negative consequences. For example, mutation of the human TER templating residues results in cell death.[41] Because the deamination rate of cytosine in single-stranded oligonucleotides is faster than that of cytosine in double-stranded duplexes,[42] the misfolded tTER would protect the coding cytosine residues.

■ CONCLUSIONS

In summary, high-resolution footprinting of protein-free and tTERT-bound tTER revealed a significant conformational change in tTER. In the absence of tTERT, tTER does not form a pseudoknot but instead forms a large stem that encompasses the pseudoknot and template nucleotides. Importantly, the data provide critical evidence that the previous solution structure models of stem II and IV derived from NMR constraints are consistent with the structure of tTERT-bound tTER, offer robust evidence for the pseudoknot structure in tTERT-bound tTER, and provide new hypotheses for telomerase RNA function during assemblage and catalysis.

■ MATERIALS AND METHODS

Preparation of tTER and pFLAG-tTERT. RNA was transcribed in vitro using Ampliscribe T7 Transcription Kit (Epicenter Technologies). Templates were generated by PCR using the plasmid pTET-telo, a pUC19-based plasmid containing the tTER gene, a T7 RNA polymerase promoter, and a self-cleaving hammerhead ribozyme that processes the 5′-end of the RNA. Primers are listed in Table S4. PCR products were gel purified using Wizard PCR Prep Kits and RNAs gel purified and stored in TE (pH 7.5) at −80 °C.

A sequence coding the FLAG epitope was ligated into a pET-28a plasmid containing tTERT cloned into the *Bam*H1 and *Xho*1 sites. Oligonucleotides were gel purified and annealed before ligation into the *Nco*1 and *Bam*H1 sites in pET-28a-tTERT. This removed the *Nco*1 site and an *Nde*1 site, allowing for easy screening of positive clones, and removed the N-terminal His- and T7-tags.

Reconstitution and Affinity Purification of Tetrahymena Telomerase. Tetrahymena telomerase was reconstituted in rabbit reticulocyte lysates following standard protocols (Promega) and affinity purified using Anti-FLAG M2 Agarose beads (Sigma). Beads were pre-washed with WB1 (20 mM Tris-acetate pH 7.5, 100 mM potassium glutamate, 5 mM $MgCl_2$, 1 mM EDTA, 0.1 mM DTT, and 10% glycerol) and blocked with blocking buffer (WB1 with 0.5 mg/mL lysozyme, 0.5 mg/mL BSA, 0.05 mg/mL glycogen, and 0.1 mg/mL yeast RNA). 400 μL of crude telomerase complex in rabbit reticulocyte lysates was mixed with 400 μL of blocking buffer, and the mixture was centrifuged at 15 000*g* for 10 min at 4 °C to remove any precipitates. The supernatant was then added to the 100 μL of pre-blocked Anti-FLAG beads, and the resultant slurry was mixed on an orbital shaker for 2 h at 4 °C. The beads were washed four times with 1400 μL of WB1 containing 300 mM potassium glutamate, two times with 1400 μL of TMG (10 mM Tris-Acetate pH 8.0, 1 mM $MgCl_2$, 0.1 mM DTT, and 10% glycerol), and resuspended in 100 μL of TMG to afford a 1:1 slurry. The telomerase complexes were eluted in 1.5 mL of Protein LoBind Tube (Eppendorf). The bead slurry containing telomerase complexes was washed two times with 1200 μL of WB2 (20 mM Tris-acetate pH 7.5, 5 mM $MgCl_2$, 1 mM EDTA, 0.1 mM DTT, and 10% glycerol). Twelve microliters of 10 mg/mL BSA was added directly to the beads, followed by 200 μL of 3xFLAG peptide solution (WB2 with 0.75 mg/mL of 3xFLAG peptide (Sigma)). This slurry was incubated on an orbital shaker for 1 h at 4 °C. The slurry was centrifuged at 1500*g* for 2 min at 4 °C, and the supernatant containing soluble telomerase was gently removed and transferred to a fresh LoBind tube. Samples were flash frozen in a dry ice/ethanol bath and stored at −80 °C.

SHAPE Analysis of tTER-3′-Ext. A 7 μL solution of tTER-3′-Ext (1 pmol) in deionized water was snap annealed by heating at 95 °C for 2 min, then cooled on ice for 5 min before 2 μL of 5× folding buffer (250 mM Hepes pH 8.0, 10 mM $MgCl_2$) was added. The solution was then incubated at 30 °C for 5 min. The RNA was then treated with 1 μL of NMIA (100 mM in anhydrous DMSO) or 1 μL of anhydrous DMSO as a control, incubated at 30 °C for 90 min, precipitated with ethanol in the presence of 0.2 M NaCl and 200 μg/mL glycogen, washed once with 70% ethanol, speed vacuumed until dry, and reconstituted in 5 μL of pH 8.0 TE buffer. Sites of modification were mapped by reverse transcription using two separate 5′-[^{32}P]-labeled primers: con-RT that binds the primer binding site in the SHAPE cassette, and C103 that binds to tTER to begin reverse transcription at C103. cDNA extension products were separated by electrophoresis and compared to dideoxythymidine sequencing ladders, visualized by phosphorimaging using ImageQuant 5.1, and quantified using SAFA. For greater detailed descritption, see the Supporting Information.

SHAPE Analysis of tTER in Complex with tTERT. Affinity purified telomerase (25 μL, ∼125 fmol) was incubated in folding buffer (50 mM Hepes pH 8.0, 2 mM $MgCl_2$) (50 μL total reaction volume) at 30 °C for 2 min. NMIA or DMSO was added to separate sample at a final concentration of 10 mM NMIA or 10% DMSO and incubated for 17.5 min (1 half-life). The reaction was immediately quenched by the addition of dithiothreitol (5 mM). The solution was proteolyzed for 10 min at 37 °C with 160 μg/mL of proteinase K in 1X TES (40 mM Tris pH 8.0, 4 mM EDTA, and 0.15% SDS), phenol/chloroform extracted, precipitated with ethanol, and reconstituted in 5 μL of RNase-Free TE pH 8.0 (Ambion). Sites of modification were mapped by reverse transcription as described above.

Structural Models of tTER. Secondary structures were modeled with SHAPE constraints using *RNAstructure*. Because *RNAstructure* could not predict the tTER pseudoknot, we compared the SHAPE reactivities to tTER pseudoknots predicted using conserved sequence analysis and heuristic folding prediction methods.

Model of tTERT. The tTERT model was generated with the crystal structure of the tTERT residues (the RNA binding domain, PDB 2R4G) and homology modeling of the remaining tTERT RT domain using the *T. castaneum* TERT crystal structure with model of the primer-template duplex bound to the active site (PDB 3KYL). The N-terminal domain of tTERT was not included. A large domain, D624−D688, in tTERT is absent in the *T. castaneum* sequence. This insertion

was modeled using ab initio folding methods and included in the tTERT model.[43] PDB 3KYL contains a RNA−DNA chimeric hairpin the mimics the template−primer duplex. Only the nucleotides representing the DNA primer were maintained in the tTERT model.

Discrete Molecular Dynamics Modeling of tTER. Sequence information and base pairs established by SHAPE were subjected to one round of refinement by DMD[23] at (T) = 0.3 for 100,000 time units (tu), where T is the reduced temperature in units of kcal/(mol·kB). After base pair formation was visually confirmed, files were prepared for incorporation of potential energy functions describing distances between FRET fluorophores. We also modeled the base pairing between tTER and a nine-nucleotide sequence complementary to the template, and a penalty for base pairing of nucleotides 10−18.

We estimated distances between four pairs of TER nucleotides using the following equation

$$\mathrm{FRET} = \frac{R_0}{R_0^6 + r^6}$$

where R_0 is the Förster radius and r is the distance between FRET fluorophores. FRET values were obtained from published single molecule FRET efficiencies between four fluorophore-labeled TER nucleotide pairs.[18b] Å Förster radius of 50 Å was used to estimate the distance between fluorophores in active telomerase observed at maximum FRET efficiency. Similarly, a Förster radius of 60 Å was used to estimate the distance between fluorophores in active telomerase observed at half-maximal FRET efficiency. It is important to note that the four labeled uridines were in full-length TER when the RNA was assembled in the telomerase complex. It is also important to note that the labeled RNAs were used by telomerase successfully as templates despite being labeled with bulky Cy3 and Cy5 adducts. We then used a potential function to restrict the distances between the four pairs of labeled TER uridines to within distances calculated from the FRET efficiencies (Figure S10).

We introduced a nine-nucleotide RNA sequence that was complementary to tTER template nucleotides 43−51 to mimic association of TER with its primer and to provide a steric block of the template from other tTER domains. The fifth nucleotide in the primer mimic was constrained to be less than 10 Å from C47. We also used a potential function to maintain the distance between nucleotides 10−18 and 38−46 to be at least 10 Å away from each other because nucleotides 15−18 are predicted to function as a protein-binding site (see Figures S10 and S11 for the potential function and algorithm used). Once constraints were incorporated, the RNA was allowed to equilibriate at T = 0.25 for 3×10^4 tu before confirming the primer mimic approached the template nucleotides. The RNA was cooled in two additional steps at T = 0.15 for 10^4 tu and T = 0.15 for 10^5 tu. One complete three-dimensional refinement of the 159 nucleotide TER required <2 h on a Linux computational node (3.2 GHz Intel Xeon IBM BladeCenter node, Red Hat Linux v5, 64-bit OS).

Distance-based hierarchical clustering was performed without user intervention on 4500 predominant RNA conformations using OC software (available at http://www.compbio.dundee.ac.uk/downloads/oc).[44] Final conformations were divided into 10 clusters, subject to the requirement that structures within a cluster agree to better than 6 Å RMSD. From the 10 clusters, we focused on the most highly populated ensemble, which contained ∼65% of the total representative models. We focused our analysis on the most central structure in each of these final clusters because the Boltzmann distribution dictates that these clusters represent the lowest free energy state. DMD model verification by RMSD alignments was computed on the basis of superposition of backbone phosphate atoms at base paired positions when compared to stem II (PDB ID 2FRL) and stem IV (PDB ID 2FEY) NMR models.

To model tTER bound to tTERT, we inserted the most populated tTER model from DMD simulations with the tTERT homology model described above. tTER was aligned with the tTERT active site by setting nucleotides 51-AAG-49 as base paired to the DNA primer. The molecular system then was relaxed with all-atom DMD simulations,[45] where the protein and template are kept fixed, and the secondary structure and FRET-based tertiary structure are maintained. The all-atom relaxation simulations were performed at room temperature (300 K). The lowest energy structure from the 100 ns simulations was used as the model structure of tTER bound to tTERT.

■ ASSOCIATED CONTENT

Ⓢ Supporting Information

Supplemental figures referred to in the text and detailed experimental methods. This material is available free of charge via the Internet at http://pubs.acs.org.

■ AUTHOR INFORMATION

Corresponding Author

jarstfer@unc.edu; dokh@unc.edu

Present Address

[○]Department of Physics and Astronomy, Clemson University, Clemson, SC 29634

Author Contributions

[§]These authors contributed equally.

Notes

The authors declare no competing financial interest.

■ ACKNOWLEDGMENTS

This work was supported by NSF grant MCB-0751372 (M.B.J.), Predoctoral fellowship 1-F31-GM086084-01 (D.I.C.), the UNC Research Council (F.D.), and NIH grant R01GM080742 (N.V.D.). We would like to thank Professor Kevin Weeks for helpful discussions.

■ REFERENCES

(1) Jacquier, A. *Nat. Rev. Genet.* **2009**, *10*, 833−44.
(2) Woodson, S. A. *Annu. Rev. Biophys.* **2010**, *39*, 61−77.
(3) Dethoff, E. A.; Chugh, J.; Mustoe, A. M.; Al-Hashimi, H. M. *Nature* **2012**, *482*, 322−30.
(4) Sekaran, V. G.; Soares, J.; Jarstfer, M. B. *Biochim. Biophys. Acta* **2010**, *1804*, 1190−1201.
(5) Fouche, N.; Moon, I. K.; Keppler, B. R.; Griffith, J. D.; Jarstfer, M. B. *Biochemistry* **2006**, *45*, 9624−31.
(6) Cech, T. R. *Cell* **2004**, *116*, 273−9.
(7) Vulliamy, T.; Marrone, A.; Goldman, F.; Dearlove, A.; Bessler, M.; Mason, P. J.; Dokal, I. *Nature* **2001**, *413*, 432−5.
(8) Donate, L. E.; Blasco, M. A. *Philos. Trans. R. Soc., B* **2011**, *366*, 76−84.
(9) Harley, C. B. *Nat. Rev. Cancer* **2008**, *8*, 167−79.
(10) Mason, M.; Schuller, A.; Skordalakes, E. *Curr. Opin. Struct. Biol.* **2011**, *21*, 92−100.
(11) (a) Robart, A. R.; O'Connor, C. M.; Collins, K. *RNA* **2010**, *16*, 563−71. (b) Sperger, J. M.; Cech, T. R. *Biochemistry* **2001**, *40*, 7005−7016.
(12) Greider, C. W.; Blackburn, E. H. *Cell* **1985**, *43*, 405−413.
(13) Collins, K.; Gandhi, L. *Proc. Natl. Acad. Sci. U.S.A.* **1998**, *95*, 8485−8490.
(14) (a) Legassie, J. D.; Jarstfer, M. B. *Structure* **2006**, *14*, 1603−9. (b) Greider, C. W.; Blackburn, E. H. *Nature* **1989**, *337*, 331−337. (c) Theimer, C. A.; Feigon, J. *Curr. Opin. Struct. Biol.* **2006**, *16*, 307−318.
(15) Collins, K. *Nat. Rev. Mol. Cell Biol.* **2006**, *7*, 484−94.
(16) (a) Mitchell, J. R.; Wood, E.; Collins, K. *Nature* **1999**, *402*, 551−5. (b) Egan, E. D.; Collins, K. *Mol. Cell. Biol.* **2010**, *30*, 2775−86.
(17) Witkin, K. L.; Collins, K. *Genes Dev.* **2004**, *18*, 1107−18.
(18) (a) Berman, A. J.; Gooding, A. R.; Cech, T. R. *Mol. Cell. Biol.* **2010**, *30*, 4965−76. (b) Stone, M. D.; Mihalusova, M.; O'Connor, C, M.; Prathapam, R.; Collins, K.; Zhuang, X. *Nature* **2007**, *446*, 458−61. (c) Singh, M.; Wang, Z.; Koo, B. K.; Patel, A.; Cascio, D.; Collins, K.; Feigon, J. *Mol. Cell* **2012**, *47*, 16−26.

(19) (a) Maida, Y.; Yasukawa, M.; Furuuchi, M.; Lassmann, T.; Possemato, R.; Okamoto, N.; Kasim, V.; Hayashizaki, Y.; Hahn, W. C.; Masutomi, K. *Nature* **2009**, *461*, 230−5. (b) Legassie, J. D.; Jarstfer, M. B. *Biochemistry* **2005**, *44*, 14191−201.
(20) Greider, C. W. *Mol. Cell. Biol.* **1991**, *11*, 4572−4580.
(21) (a) McCormick-Graham, M.; Romero, D. P. *Nucleic Acids Res.* **1995**, *23*, 1091−1097. (b) Chen, J.-L.; Blasco, M. A.; Greider, C. W. *Cell* **2000**, *100*, 503−514.
(22) Wilkinson, K. A.; Merino, E. J.; Weeks, K. M. *Nat. Protoc.* **2006**, *1*, 1610−6.
(23) Ding, F.; Sharma, S.; Chalasani, P.; Demidov, V. V.; Broude, N. E.; Dokholyan, N. V. *RNA* **2008**, *14*, 1164−73.
(24) Mitchell, M.; Gillis, A.; Futahashi, M.; Fujiwara, H.; Skordalakes, E. *Nat. Struct. Mol. Biol.* **2010**, *17*, 513−8.
(25) Rouda, S.; Skordalakes, E. *Structure* **2007**, *15*, 1403−12.
(26) McGinnis, J. L.; Dunkle, J. A.; Cate, J. H.; Weeks, K. M. *J. Am. Chem. Soc.* **2012**, *134*, 6617−24.
(27) Deigan, K. E.; Li, T. W.; Mathews, D. H.; Weeks, K. M. *Proc. Natl. Acad. Sci. U.S.A.* **2009**, *106*, 97−102.
(28) (a) Chen, Y.; Fender, J.; Legassie, J. D.; Jarstfer, M. B.; Bryan, T. M.; Varani, G. *EMBO J.* **2006**, *25*, 3156−66. (b) Richards, R. J.; Theimer, C. A.; Finger, L. D.; Feigon, J. *Nucleic Acids Res.* **2006**, *34*, 816−25. (c) Richards, R. J.; Wu, H.; Trantirek, L.; O'Connor, C.; Collins, M.; Feigon, K. J. *RNA* **2006**, *12*, 1475−1485.
(29) Gherghe, C. M.; Shajani, Z.; Wilkinson, K. A.; Varani, G.; Weeks, K. M. *J. Am. Chem. Soc.* **2008**, *130*, 12244−5.
(30) Bhattacharyya, A.; Blackburn, E. H. *EMBO J.* **1994**, *13*, 5721−31.
(31) Mihalusova, M.; Wu, J. Y.; Zhuang, X. *Proc. Natl. Acad. Sci. U.S.A.* **2011**, *108*, 20339−44.
(32) Romero, D. P.; Blackburn, E. H. *Cell* **1991**, *67*, 343−53.
(33) Lu, Z. J.; Gloor, J. W.; Mathews, D. H. *RNA* **2009**, *15*, 1805−13.
(34) Bellaousov, S.; Mathews, D. H. *RNA* **2010**, *16*, 1870−80.
(35) Ulyanov, N. B.; Shefer, K.; James, T. L.; Tzfati, Y. *Nucleic Acids Res.* **2007**, *35*, 6150−60.
(36) (a) Cao, S.; Giedroc, D. P.; Chen, S. J. *RNA* **2010**, *16*, 538−52. (b) Sato, K.; Kato, Y.; Hamada, M.; Akutsu, T.; Asai, K. *Bioinformatics* **2011**, *27*, i85−93. (c) Ren, J.; Rastegari, B.; Condon, A.; Hoos, H. H. *RNA* **2005**, *11*, 1494−504. (d) Bindewald, E.; Kluth, T.; Shapiro, B. A. *Nucleic Acids Res.* **2010**, *38*, W368−72.
(37) (a) Ding, F.; Lavender, C. A.; Weeks, K. M.; Dokholyan, N. V. *Nat. Methods* **2012**, *9*, 603−8. (b) Gherghe, C. M.; Leonard, C. W.; Ding, F.; Dokholyan, N. V.; Weeks, K. M. *J. Am. Chem. Soc.* **2009**, *131*, 2541−6. (c) Cruz, J. A.; Blanchet, M. F.; Boniecki, M.; Bujnicki, J. M.; Chen, S. J.; Cao, S.; Das, R.; Ding, F.; Dokholyan, N. V.; Flores, S. C.; Huang, L.; Lavender, C. A.; Lisi, V.; Major, F.; Mikolajczak, K.; Patel, D. J.; Philips, A.; Puton, T.; Santalucia, J.; Sijenyi, F.; Hermann, T.; Rother, K.; Rother, M.; Serganov, A.; Skorupski, M.; Soltysinski, T.; Sripakdeevong, P.; Tuszynska, I.; Weeks, K. M.; Waldsich, C.; Wildauer, M.; Leontis, N. B.; Westhof, E. *RNA* **2012**, *18*, 610−25.
(38) (a) Cunningham, D. D.; Collins, K. *Mol. Cell. Biol.* **2005**, *25*, 4442−54. (b) Lai, C. K.; Mitchell, J. R.; Collins, K. *Mol. Cell. Biol.* **2001**, *21*, 990−1000.
(39) (a) Autexier, C.; Greider, C. W. *Nucleic Acids Res.* **1998**, *26*, 787−795. (b) Licht, J. D.; Collins, K. *Genes Dev.* **1999**, *13*, 1116−1125.
(40) Berman, A. J.; Akiyama, B. M.; Stone, M. D.; Cech, T. R. *Nat. Struct. Mol. Biol.* **2011**, *18*, 1371−5.
(41) Kim, M. M.; Rivera, M. A.; Botchkina, I. L.; Shalaby, R.; Thor, A. D.; Blackburn, E. H. *Proc. Natl. Acad. Sci. U.S.A.* **2001**, *98*, 7982−7.
(42) Frederico, L. A.; Kunkel, T. A.; Shaw, B. R. *Biochemistry* **1990**, *29*, 2532−7.
(43) Sharma, S.; Ding, F.; Nie, H.; Watson, D.; Unnithan, A.; Lopp, J.; Pozefsky, D.; Dokholyan, N. V. *Bioinformatics* **2006**, *22*, 2693−4.
(44) Barton, G. J. O.-A., 2002; www.compbio.dundee.ac.uk/downloads/oc.
(45) Ding, F.; Tsao, D.; Nie, H.; Dokholyan, N. V. *Structure* **2008**, *16*, 1010−8.